Electronic Supplementary Information (ESI) for

Ni(II)MOF based hypersensitive dual-function luminescent sensor towards 3-nitrotyrosine biomarker and 6-propyl-2-thiouracil antithyroid drug in urine

Wencui Li[a,†], Liying Liu[a,†], Xiaoting Li[a], Hu Ren[a], Lu Zhang[a], Mohammad Khalid Parvez[c], Mohammed S. Al-Dosari[c], Liming Fan[*a] and Jianqiang Liu[*b]

[a] *School of Chemistry and Chemical Engineering, North University of China, Taiyuan 030051, P. R. China.*

[b] *Dongguan Key Laboratory of Drug Design and Formulation Technology, Guangdong Provincial Key Laboratory of Medical Molecular Diagnostics, Guangdong Medical University, Dongguan 523000, P. R. China.*

[c] *Department of Chemistry, College of Sciences, King Saud University, Riyadh 11451, Saudi Arabia.*

E-mail:limingfan@nuc.edu.cn; jianqiangliu8@gdmu.edu.cn.

Table of Contents

Materials and Methods. H_2L, selected analytes, as well as all other starting reagents are readily obtainable from commercial sources and were utilized directly. The EA-1110 elemental analyzer is utilized for conducting the elemental analysis of carbon, oxygen, and hydrogen. FT-IR spectrum was captured precisely using a Nicolet NEXUS-670 FT-IR spectrometer, employing the KBr pellet. TG-DTG curve was acquired *via* a PerkinElmer DTA-6000 synchronous thermal analyzer, encompassing a temperature range from 30°C to 800°C under N_2 atmosphere, with a gradual heating rate of 10°C per minute.PXRD data were comprehensively gathered using a Rigaku D/Max-2500 PC diffractometer (λ=1.5418 Å). UV–vis diffuse reflectance spectrawere gathered utilizinga JASCO V-750 spectrophotometer. Additionally, luminescent spectrawere collected by a Hitachi F-4600 spectrophotometer, with a 450 W Xenon lamp asexcitation source.

Preparation of $\{[Ni_3(L)_3(\mu_2\text{-}H_2O)]\cdot 6H_2O\cdot 2DMA\}_n$ (NiMOF). A mixture comprising 0.02 mmol H_2L,0.06 mmol $NiCl_2\cdot 6H_2O$, 2 mL acetonitrile, 3 mL DMA, and 3 mL H_2O were sequentially added into the PTFE lining of 25 mL stainless steel reaction and heated at 120°C for 3 days. After cooled to room temperature at a 10 °C/h decreasing rate, the greenblock crystals of NiMOF were obtained with a 39 % yield (based on H_2L). Anal. Calcd for $C_{56}H_{70}N_2Ni_3O_{28}$: C, 48.21; N, 2.01; H, 5.06. Found: C, 48.52; N, 1.98; H, 5.19. IR (KBr, cm^{-1}): 3428(w), 2825(w), 2360(w), 1623 (vs), 1394 (vs), 1182 (w), 1008 (w), 782 (s), 678 (s).

X-ray Crystallography. A flawless, green block crystal of NiMOF was diligently chosen and performed to a Rigaku XtaLAB Synergy diffractometer to acquire single-crystal X-ray diffraction data through the utilization of Mo-Kα radiation (λ=0.71073 Å) at 150 K. Subsequently, the crystal structure of NiMOF was analyzed and refined with the assistance of the SHELXL-2018/3 package. Free solvents were omitted and were determined based on the results of EA and TGA. Due to the flexible backbone of H_2L ligand, related carbon atomsexhibited disorder, necessitating refinement with an occupancy ratio of 86:14 for C8, C9 and C8′, C9′, and 38.3:61.7 for C18-C24 and C18′-C24′, respectively. Refined cif file of NiMOF has been deposited at https://ccdc.cam.ac.uk, with the CCDC number is 2370376. Table S2 provides comprehensive crystallographic data and details of the NiMOF crystal structure. Additionally, the Ni-O bond distances and select bond angles of NiMOF were listed in Table S3.

Luminescent Sensing Operation. Initially, the preparation of the tested samples involved the incorporation of 1 mg of thoroughly ground NiMOF powder into 2 mL aqueous solutions containing 10 mM urine species of ammonium chloride (NH_4Cl), urea, potassium chloride (KCl), uric acid (UA), calcium chloride ($CaCl_2$), cysteine (Cys), creatinine (Crea), Creatine (Cre), sodium chloride (NaCl), glucose (Gluc), magnesium chloride ($MgCl_2$), phenylalanine (Phe), histidine (His), 3-NT biomarker, and antithyroid drug of 6-PTU. Subsequently, the luminescent sensing capabilities of these analytes in the NiMOF suspensions were evaluated using a Hitachi F-4600 spectrophotometer. Furthermore, gradient titration experiments were conducted in water and 100-fold diluted urine by adding varying volumes of 3-NT or 6-PTU into the NiMOF suspensions, and corresponding response emission spectra were recorded. Additionally, to evaluate the anti-interference capabilities of NiMOF in detecting 6-PTU and 3-NT, equimolar concentrations of interfering species were introduced into NiMOF suspensions containing 10 mM of the target analytes. Lastly, the reusability of NiMOF in detecting 6-PTU and 3-NT was assessed by utilizing recycled NiMOF samples that had undergone filtration, washing, and drying procedures.

Table S1 Comparative performances of MOFs-based luminescent sensors in detecting 3-NT biomarker.

	MOFs Based Sensor	K_{sv} (M^{-1})	LOD (μM)	Media	Reference
1	HfMOF	3.10×10^4	0.54	HEPES solution	42
2	ZnMOF	6.59×10^4	0.31	H_2O	43
3	CdMOF	9.58×10^4	0.43	H_2O	44
4	CoMOF-1	9.19×10^4	0.10	PBS solution	45
5	CoMOF-2	1.05×10^5	0.09	PBS solution	
6	CuMOF	1.94×10^4	0.49	H_2O	46
7	NiMOF	1.42×10^5	0.17	H_2O	35
8	NiMOF	3.11×10^4	0.31	H_2O	This work

Table S2 Crystal data of NiMOF.

Empirical formula	$C_{48}H_{40}Ni_3O_{20}$
Formula weight	1112.93
Crystal system	monoclinic
Space group	C2/c
a [Å]	23.2911(15)
b [Å]	18.3233(11)
c [Å]	16.5576(9)
α (°)	90
β [º]	104.174(2)
γ (°)	90
V [Å^3]	6851.2(7)
Z	4
*D*c/(g·cm^{-3})	1.078
F(000)	2288
μ(Mo *K*α)/mm^{-1}	0.872
Data/restraints/parameters	7044/391/422
R_{int}	0.0774
Goodness-of-fit on F^2	1.073
R_1, $wR_2[I>2\sigma(I)]$	0.0438, 0.1062
R_1, wR_2(all data)	0.0638, 0.1143
CCDC number	2370376

Table S3 Selected bond lengths (Å) and angles (º) of NiMOF.

Ni(1)-O(5)	2.067(2)	O(5)-Ni(1)-O(6)	83.72(9)	O(2)-Ni(2)-O(1W)$^{\#6}$	89.03(7)
Ni(1)-O(6)	2.070(2)	O(5)-Ni(1)-O(4)$^{\#1}$	92.53(9)	O(9)$^{\#3}$-Ni(2)-O(1W)$^{\#6}$	91.28(8)
Ni(1)-O(4)$^{\#1}$	2.0795(19)	O(6)-Ni(1)-O(4)$^{\#1}$	176.09(9)	O(9)$^{\#4}$-Ni(2)-O(1W)$^{\#6}$	93.60(8)
Ni(1)-O(1)	2.0812(18)	O(5)-Ni(1)-O(1)	95.79(10)	O(2)-Ni(2)-O(2)$^{\#2}$	92.85(10)
Ni(1)-O(8)	2.0853(19)	O(6)-Ni(1)-O(1)	89.68(8)	O(2)-Ni(2)-O(9)$^{\#3}$	92.13(8)
Ni(1)-O(7)	2.1886(19)	O(4)$^{\#1}$-Ni(1)-O(1)	91.82(7)	O(2)$^{\#2}$-Ni(2)-O(9)$^{\#3}$	174.50(8)
Ni(2)-O(2)$^{\#2}$	2.0841(17)	O(5)-Ni(1)-O(8)	167.95(10)	O(2)-Ni(2)-O(9)$^{\#4}$	174.51(8)
Ni(2)-O(2)$^{\#2}$	2.0841(17)	O(6)-Ni(1)-O(8)	91.98(8)	(2)$^{\#2}$-Ni(2)-O(9)$^{\#4}$	92.13(8)
Ni(2)-O(9)$^{\#3}$	2.090(2)	O(4)$^{\#1}$-Ni(1)-O(8)	91.47(8)	O(9)$^{\#3}$-Ni(2)-O(9)$^{\#4}$	82.99(12)
Ni(2)-O(9)$^{\#4}$	2.090(2)	O(1)-Ni(1)-O(8)	95.44(7)	O(2)-Ni(2)-O(1W)$^{\#5}$	86.48(7)
Ni(2)-O(1)$^{\#5}$	2.1349(19)	O(5)-Ni(1)-O(7)	107.18(10)	O(2)$^{\#2}$-Ni(2)-O(1W)$^{\#5}$	89.03(7)
Ni(2)-O(1)$^{\#6}$	2.1349(19)	O(6)-Ni(1)-O(7)	92.57(9)	O(9)$^{\#3}$-Ni(2)-O(1W)$^{\#5}$	93.60(8)
		O(4)$^{\#1}$-Ni(1)-O(7)	87.45(8)	O(9)$^{\#4}$-Ni(2)-O(1W)$^{\#5}$	91.28(8)
		O(1)-Ni(1)-O(7)	157.02(7)	O(2)$^{\#2}$-Ni(2)-O(1W)$^{\#6}$	86.47(7)
		O(8)-Ni(1)-O(7)	61.64(7)	O(1W)$^{\#5}$-Ni(2)-O(1W)$^{\#6}$	173.48(9)

Symmetry codes:#1 0.5-x, -0.5+y, 1.5-z; #2 -x, y, 0.5-z; #3 x, 1+y, z; #4 -x, 1+y, 0.5-z; #5 x, 1-y, -0.5+z; #6x, 1-y, -0.5+z.

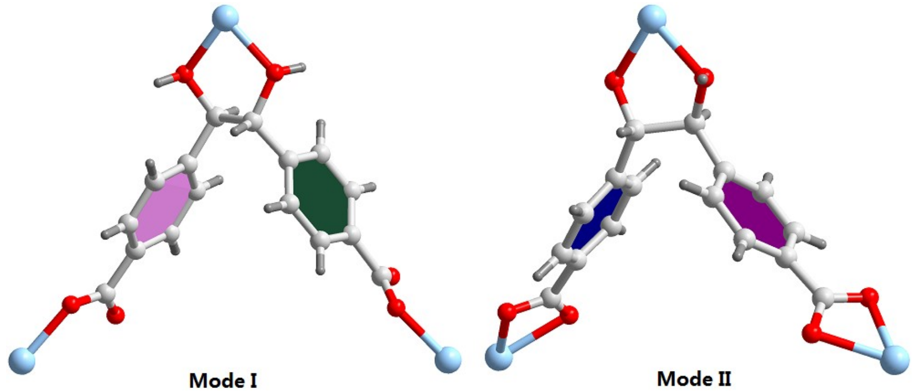

Fig. S1 The coordination modes of H_2L in the assembly of NiMOF.

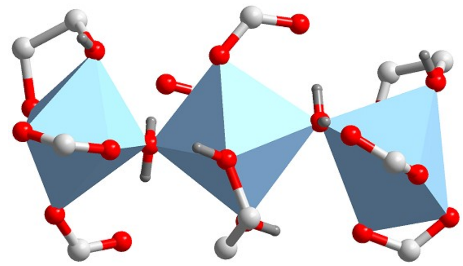
Fig. S2 The trinuclear cluster in NiMOF.

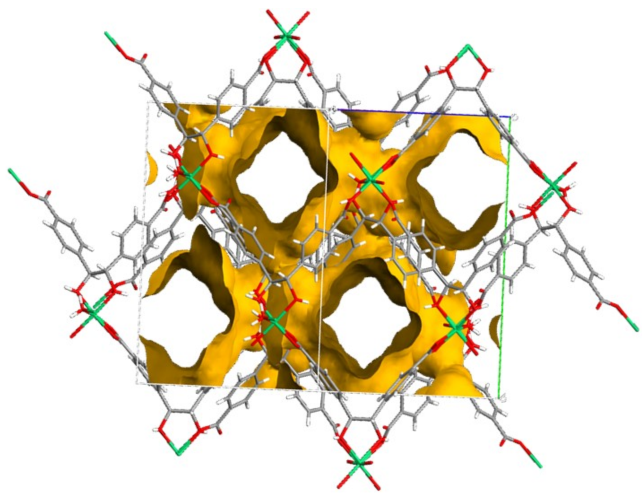
Fig. S3 The 3D porous framework of NiMOF with the sugarcoated haws shaped channels.

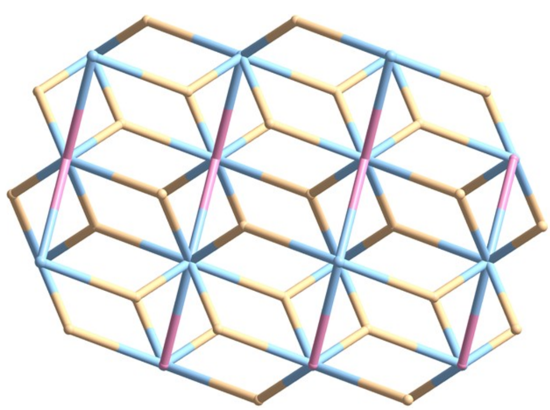
Fig. S4 The simplified 3,9-c$\{4^2.6\}_3\{4^6.6^{21}.8^9\}$-xmz net for NiMOF.

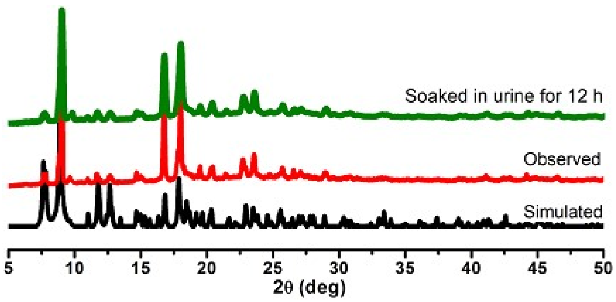

Fig. S5 PXRD patterns of NiMOF.

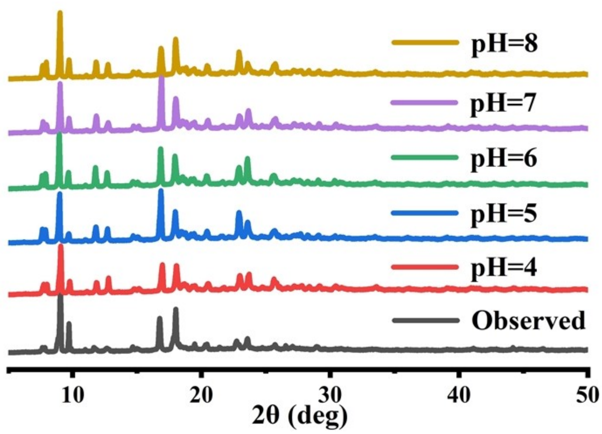

Fig. S6 PXRD patterns of NiMOF after immersed in aqueous solution with different pH values for 12 hours.

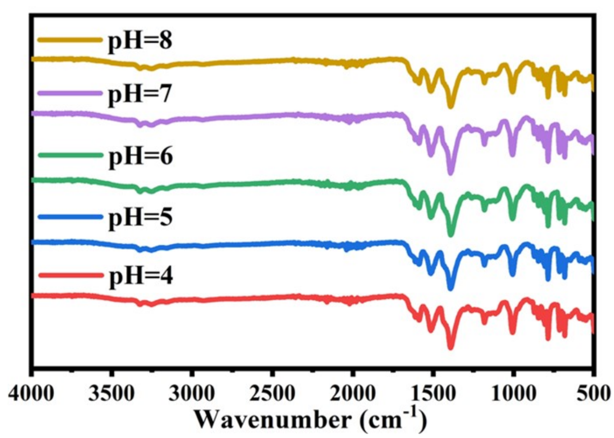

Fig. S7 FT-IR spectra of NiMOF immersed in aqueous solution with different pH values for 12 hours.

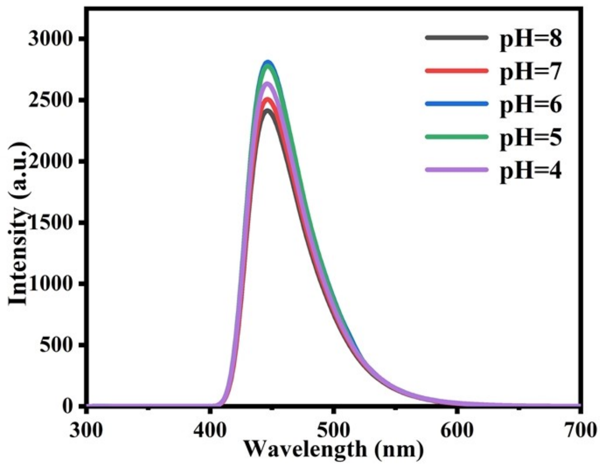

Fig. S8 Emission spectra of NiMOF suspensions in aqueous solutions at pH = 4-8.

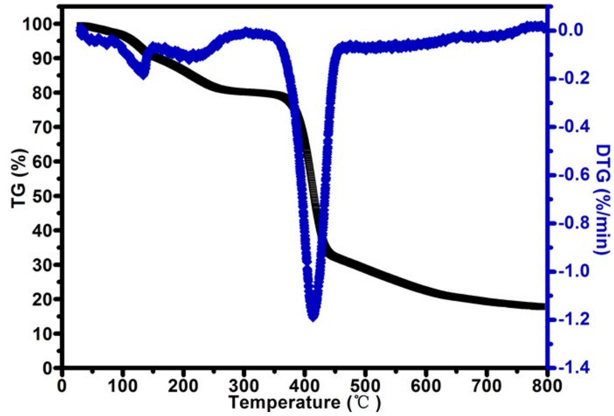

Fig. S9 TG-DTG curve of NiMOF.

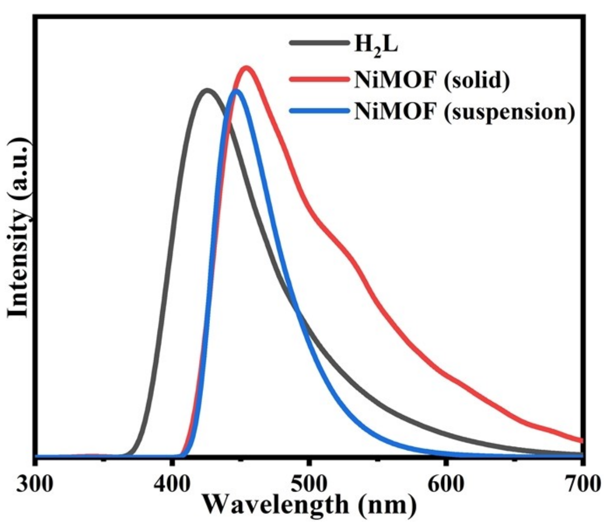

Fig. S10 Luminescence of H_2L and NiMOF.

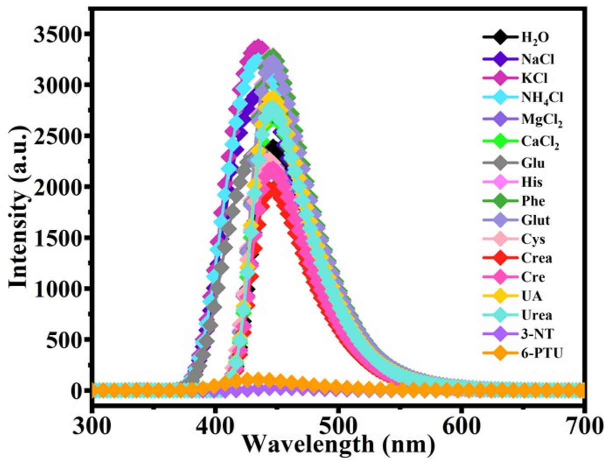

Fig. S11 Emission spectra of NiMOF suspensions in aqueous solution containing 10 mM urine analytes.

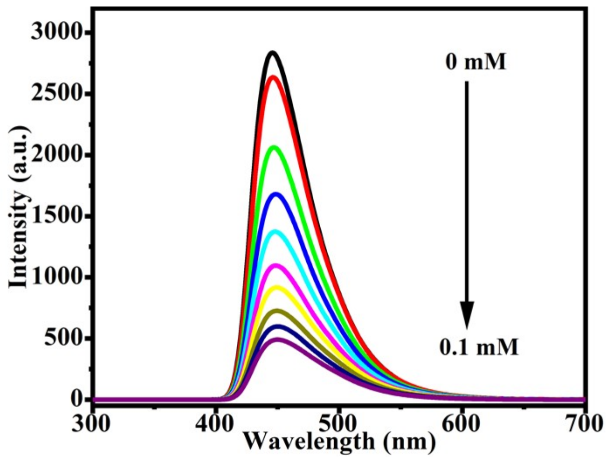

Fig. S12 Emission spectra of the suspensions of NiMOF by gradual addition of 3-NT.

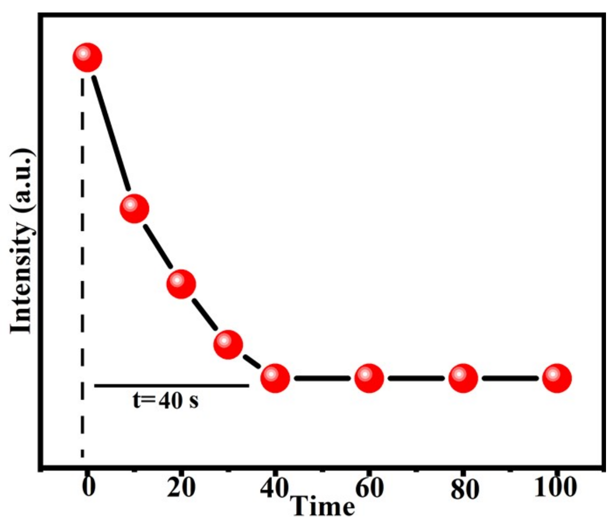

Fig. S13 The response time of NiMOF in sensing 3-NT in aqueous solutions.

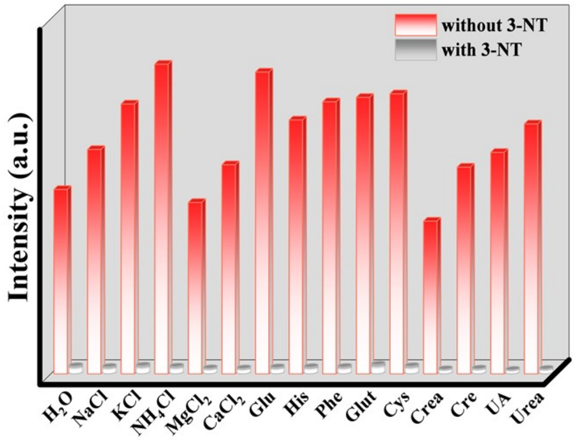

Fig. S14 Anti-interference performance of NiMOF in sensing 3-NT in aqueous solutions.

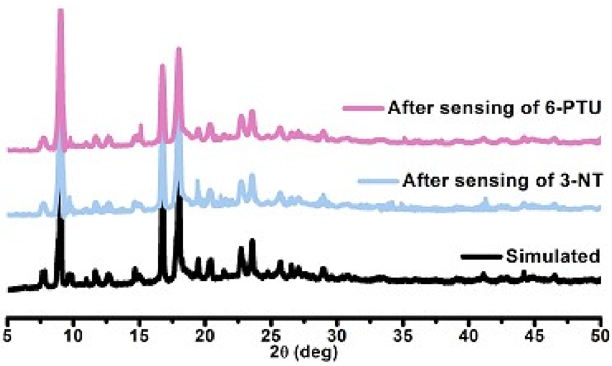

Fig.S15 PXRD patterns of NiMOF after 5 cycles sensing 3-NT and 6-PTU.

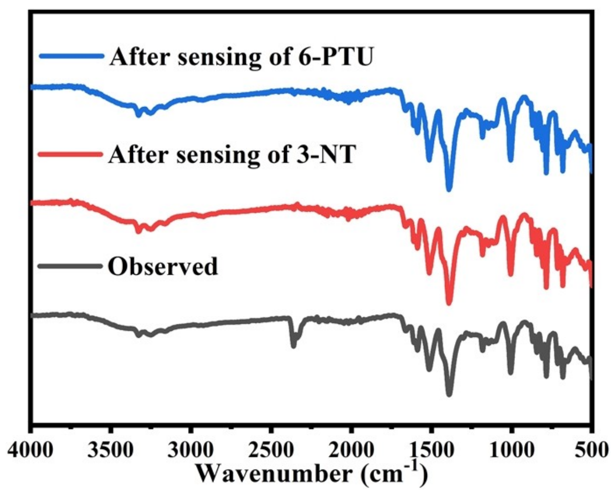

Fig. S16 FT-IR spectra of NiMOF after 5 cycles sensing 3-NT and 6-PTU.

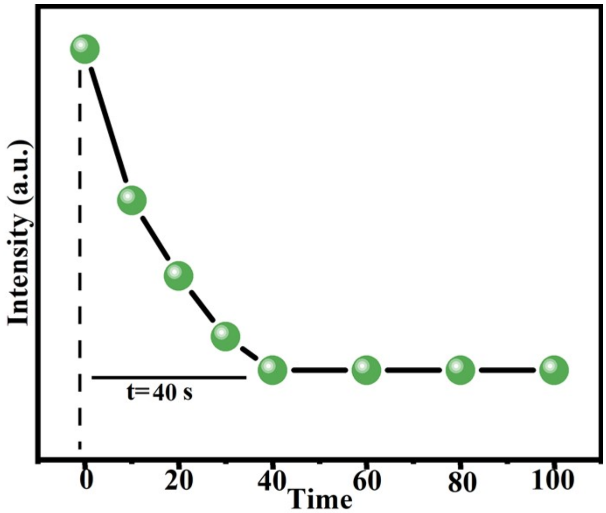

Fig. S17 The response time of NiMOF in sensing 6-PTU in aqueous solutions.

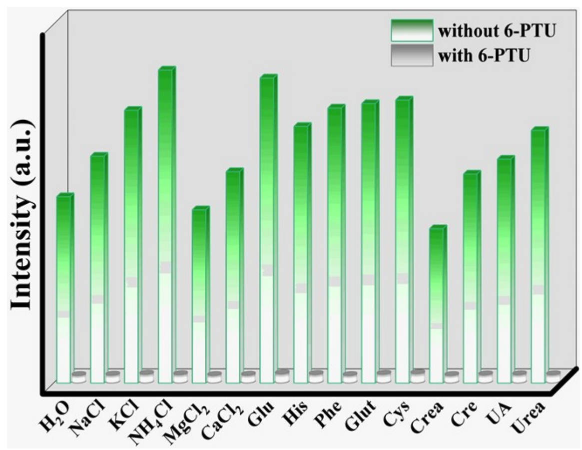

Fig. S18 Anti-interference performance of NiMOF in sensing 6-PTU in aqueous solutions.

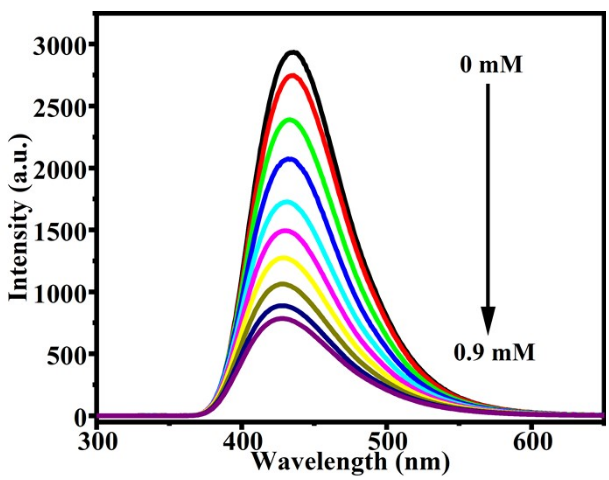

Fig. S19 Emission spectra of the suspensions of NiMOF by gradual addition of 6-PTU.

Gate 1

Input 1		Output 1
$C_{6\text{-}PTU}$	λ_{EX}=336nm	
0	0	0
1	0	0
0	1	0
1	1	1

Gate 2

Input 2			Output 2
$C_{6\text{-}PTU}$	λ_{EX}=336nm	Output 1	
0	0	0	0
1	0	0	0
0	1	0	0
1	1	0	0
0	0	1	0
1	0	1	0
0	1	1	0
1	1	1	1

Gate 3

Input 3			Output 3
$C_{6\text{-}PTU}$	λ_{EX}=336nm	Output 2	
0	0	0	0
1	0	0	0
0	1	0	0
1	1	0	0
0	0	1	0
1	0	1	0
0	1	1	0
1	1	1	1

Fig. S20 The truth table of Gate 1, Gate 2 and Gate 3 in 6-PTU detection.

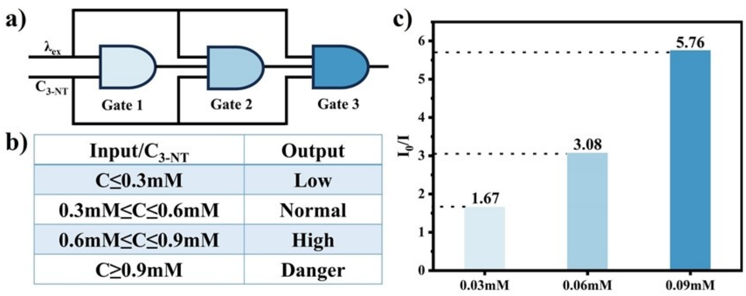

Fig. S21 (a) The electronic equivalent circuit utilizing tandem combinational logic gates of 3-NT. (b) Threshold histograms depicting the relative luminescence intensity (I_0/I) for each individual logic gate of 3-NT. (c) Output signals aligned with varying $C_{3\text{-}NT}$ inputs.

Gate 1

Input 1		Output 1
λ_{ex}	$C_{3\text{-}NT}$	
0	**0**	**0**
0	**1**	**0**
1	**0**	**0**
1	**1**	**1**

Gate 2

Input 2			Output 2
λ_{ex}	$C_{3\text{-}NT}$	Output 1	
0	**0**	**0**	**0**
0	**1**	**0**	**0**
1	**0**	**0**	**0**
0	**0**	**1**	**0**
1	**0**	**1**	**0**
1	**1**	**0**	**0**
0	**1**	**1**	**0**
1	**1**	**1**	**1**

Gate 3

Input 3			Output 3
λ_{ex}	$C_{3\text{-}NT}$	Output 2	
0	**0**	**0**	**0**
0	**1**	**0**	**0**
1	**0**	**0**	**0**
0	**0**	**1**	**0**
1	**0**	**1**	**0**
1	**1**	**0**	**0**
0	**1**	**1**	**0**
1	**1**	**1**	**1**

Fig. S22 The truth table of Gate 1, Gate 2 and Gate 3 in 3-NT detection.